NANO LETTERS

pubs.acs.org/NanoLett

Letter

Plasmonic Lithium Niobate Mach–Zehnder Modulators

Martin Thomaschewski,* Vladimir A. Zenin, Saskia Fiedler, Christian Wolff, and Sergey I. Bozhevolnyi

Cite This: *Nano Lett.* 2022, 22, 6471–6475

Read Online

ACCESS | Metrics & More | Article Recommendations | Supporting Information

ABSTRACT: Lithium niobate Mach–Zehnder modulators (MZMs) are present in a wide range of technologies and though fulfilling the performance and reliability requirements of present applications, they are becoming progressively too bulky, power inefficient, and slow in switching to keep pace with future technological demands. Here, we utilize plasmonics to demonstrate the most efficient ($V_\pi L$ = 0.23 Vcm) lithium niobate MZM to date, consisting of gold nanostripes on lithium niobate that guide both plasmonic modes and electrical signals that control their relative optical phase delay, thereby enabling efficient electro-optic modulation. For high linearity (modulation depth of >2 dB), the proposed MZM inherently operates near its quadrature point by shifting the relative phase of the signal in the interferometric arms. The demonstrated lithium niobate MZM manifests the benefits of employing plasmonics for applications that demand compact (<1 mm^2) and fast (>10 GHz) photonic components operating reliably at ambient temperatures.

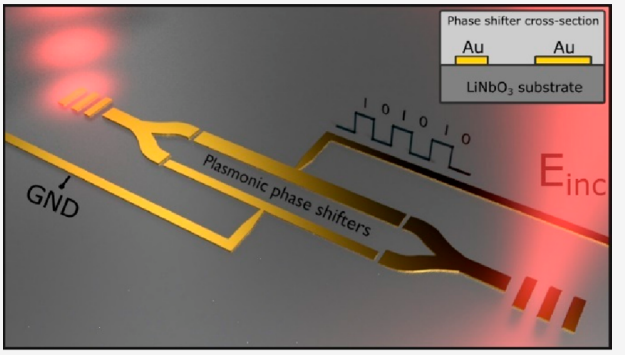

KEYWORDS: *Surface plasmon polaritons, Pockels effect, optoelectronics, nanophotonics, integrated optics*

Mach–Zehnder Modulators (MZM) are key devices for electric-to-optical conversion in integrated photonics, telecommunications, and sensing.[1−4] In an integrated MZI modulator, a guided light beam is split into two paths and a phase difference between the two waveguide arms is induced using an electro-optically active material, most commonly lithium niobate (LN, $LiNbO_3$) due to its preferential physical properties, such as moderate and stable electro-optic activity (~30 pm V^{-1}) and wide optical transparency (0.35–4.5 μm).[5] The phase difference in the waveguides results in a modulation of the output intensity by letting the phase-shifted beam interfere with a reference beam when the two waveguides are combined. Major performance limiting factors in terms of modulation bandwidth, modulation depth, energy per bit and footprint of an MZM are determined by the electro-optic efficiency of the phase-shifters.[6] As photonic technology utilizes poorly confined optical waveguides (titanium-indiffused or proton-exchanged in bulk LN)[7−9] which are limiting the electro-optic interaction, the efficiency of conventional MZM remains low. Thin-film lithium niobate modulators[10−15] lead to improvements in terms of compactness, operation speed and energy efficiency, while still demanding relatively long (on the mm scale) interaction lengths due to fundamental limitations in the achievable overlap between the optical and modulating electric fields.

Plasmonic lithium niobate technology[16,17] has recently emerged as a strong contender to overcome current performance limitations by providing electro-optic phase shifters with the highest efficiency ever reported in a lithium niobate device. Because of the ultrafast Pockels effect (with a response time in the order of femtoseconds[19]) utilized in plasmonic lithium niobate devices with high modulation efficiency characterized by a voltage-length product as low as $V_\pi L$ = 0.21 Vcm, small device footprints with increased operation bandwidths far beyond 100 GHz are enabled. Among the demonstrated performance improvements in plasmonic lithium niobate devices, the implementation of an MZM which utilizes the extremely high modulation efficiency in plasmonic lithium niobate phase shifters remained unexplored and has yet to be demonstrated.

Here, we utilize the plasmonic lithium niobate platform to enable an efficient ($V_\pi L$ = 0.23 Vcm) and fast (≥10 GHz) integrated MZM formed by phase shifters consisting of two only 15 μm long plasmonic strip waveguides which supports both the optical signals converted to surface plasmon polaritons (SPPs) propagating at metal–dielectric interfaces and the electrical signal introducing the electro-optically induced phase shift.[20−25] The extreme confinement of the corresponding optical and electrostatic fields and the large overlap between the corresponding fields opens a path for novel highly efficient lithium niobate MZM.

Received: February 21, 2022
Revised: July 22, 2022
Published: August 11, 2022

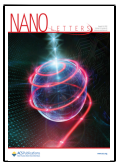

https://doi.org/10.1021/acs.nanolett.2c00714
Nano Lett. 2022, 22, 6471–6475

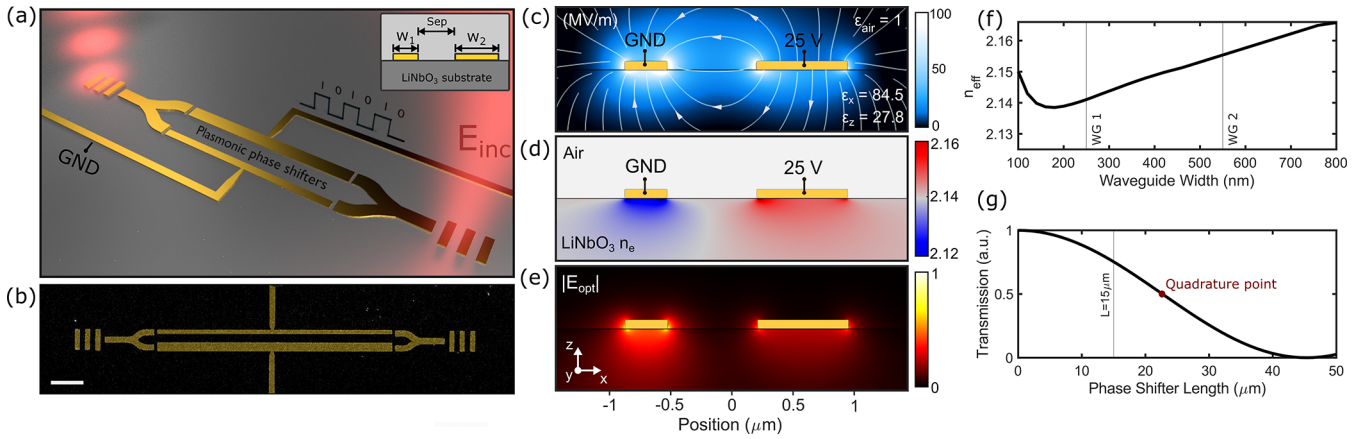

Figure 1. Plasmonic lithium niobate unbalanced MZM. (a) Conceptional image of electro-optic modulation in the MZM. The inset shows the cross-section of two parallel waveguides with the width of w_1 = 250 nm and w_2 = 550 nm, separated by 550 nm and placed on bulk *z*-cut lithium niobate (LN, $LiNbO_3$) substrate. (b) False-colored scanning electron microscope (SEM) image of an investigated MZM. The scalebar represents 2 μm. (c) Color-coded electric field and its contours upon applying a bias of 25 V. (d) Change of the extraordinary refractive index n_e due to the electro-optic (linear) Pockels effect in lithium niobate. (e) The optical field distribution of the antisymmetric mode overlaps with the electro-optically induced change of the refractive index in LN. (f) Mode effective index n_{eff} as a function of the waveguide width. (g) Transfer function for the MZM with 15 μm phase-shifter length.

The studied asymmetric plasmonic lithium niobate MZM is based on two subwavelength gold nanowires as active phase shifter which are connected to two Y-branches serving as integrated waveguide splitter and combiner (Figure 1). Each gold nanowire supports the propagation of SPP modes guided along the nanowire with subwavelength field confinement,[26−28] thereby acting as an ultracompact waveguide in the nanophotonic integrated circuit. The plasmonic mode is launched by positioning a diffraction-limited beam (λ_0 = 1550 nm) on the terminating metallic grating coupler with a calculated coupling efficiency of 10% at the wavelength of λ_0 = 1550 nm. The mode is split by an integrated branch junction, which feeds the two active phase shifters by a 150 nm wide isolating air gap. The two 15 μm long waveguides of the phase shifter section have different widths, that is, one waveguide has the width of w_1 = 250 nm while the other has the width of w_1 = 550 nm, and they are separated by edge-to-edge separation distance of g = 550 nm. Because of the dependence of the waveguide geometry on the mode effective index of the supporting plasmonic mode (Figure 1f), the operation point of the MZM is passively shifted near the quadrature point (Figure 1g). This asymmetric configuration thereby offers high degree of modulation linearity at the operation regime of the MZM and the collapse of nonlinear distortions in the modulation spectrum. The refractive index of lithium niobate is modulated by applying a voltage across the two parallel wires comprising the plasmonic waveguides, and therefore the phase of the plasmonic modes propagating along them is shifted. Because of the Pockels effect in LN, the refractive index changes linearly to the applied electric field. The largest electro-optic coefficient r_{33} is along the optic axis of the LN crystal. Therefore, the electrical field E_z along the out-of-plane direction results in the strongest change of the extraordinary refractive index n_e in *z*-cut LN, according to $\Delta n_e(E_z) \approx -0.5 r_{33} n_e^3 E_z$. Considering the electric field distribution $E(x, z)$ when the wires are biased (Figure 1c), the change of the refractive index is mainly located underneath the Au nanowires with an opposite modification between the individual wires due to an opposite direction of the electric field. The large overlap between the modification of the refractive index and the optical field distribution results in a significant phase change with opposite directions in the two optical channels (push−pull phase modulation). Because of a different waveguide geometry, the strength of the electro-optic interaction is nonidentical for the two individual phase shifters. The optical mode and the electrostatic field are stronger confined in the narrower waveguide (w_1 = 250 nm) resulting in a higher modulation efficiency, characterized by the calculated voltage-length product of 0.37 Vcm, compared to the wider phase shifter waveguide (w_2 = 550 nm) exhibiting a voltage-length product of 0.57 Vcm. As the MZM inherently introduces phase shifts in push−pull operation, the voltage-length product of the device is reduced to 0.23 Vcm (Figure 1c-e). For the electrical isolation between the two individual phase shifter waveguides, isolating gaps between the phase shifters and the Y-branches are required. The separation between the waveguides is designed to be large enough to prevent parasitic directional coupling between the nonidentical waveguides (Supporting Information Note S2). Furthermore, the isolating gap between the phase shifters and the Y-branch is small enough ($g \ll \lambda_{SPP}$) to allow optical transmission through the air gap. The scattering losses are characterized as a function of the gap size (Figure 2). For the nominal gap size of 150 nm, which is much smaller than the wavelengths $\lambda_{SPP,1}$ = 725 nm (w_1 = 250 nm) and $\lambda_{SPP,2}$ = 720 nm (w_2 = 550 nm) of the SPPs propagating along the phase shifters, an optical loss of ∼3.5 dB per isolating gap is estimated. Furthermore, the propagation loss is investigated by an array of single waveguides with different length. The propagation loss in a 15 μm long and 350 nm wide waveguide is estimated to be 19.5 dB, which indicate much higher losses than expected from simulations (0.35 dB/μm) and are likely attributed to additional losses due to the titanium adhesion layer and the grain boundaries of the polycrystalline gold nanowires.

The proposed MZM device is characterized by positioning a focused linearly polarized beam (λ_0 = 1550 nm) onto the grating coupler at normal incidence (Supporting Information Note S1). The SPPs are launched and feed the phase shifters at the interferometric arms of the MZM before the signals interfere at the opposite Y-branch. For obtaining the Mach−Zehnder transfer function, the scattering signal of the output

https://doi.org/10.1021/acs.nanolett.2c00714
Nano Lett. 2022, 22, 6471−6475

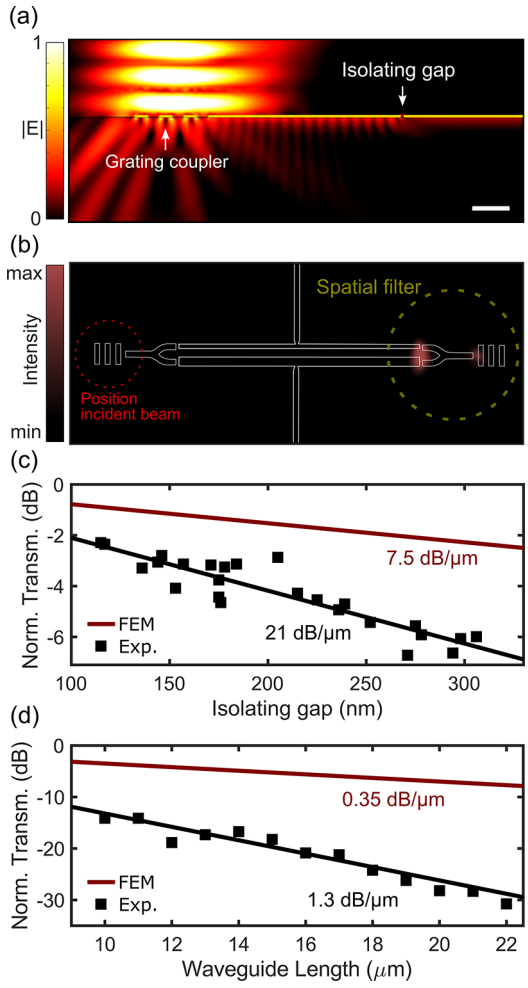

Figure 2. Investigation of the optical losses in a single plasmonic waveguide consisting of a 50 nm thick stripe and an air gap for electric isolation. (a) Electric field distribution simulated for a waveguide with grating coupler and isolating gap of 100 nm. (b) Experimental optical far-field image captured by an infrared camera with a spatial filter at the output port. The laser beam (λ_0 = 1.55 μm) is positioned on the left grating coupler with its reflection being blocked in front of the camera to prevent image overexposure. The structure design is superimposed as a guide to the eye. (c) Measured normalized transmission as a function of the width of the isolating gap. (d) Measured waveguide transmission as a function of the waveguide length without an isolating gap.

grating is spatially filtered and detected with an infrared photodiode. The voltage-dependent output intensity follows the expected transfer function of an unbalanced MZM exhibiting a passive phase shift of 0.28π (Figure 3a). Continuous, robust, and quasi-linear intensity modulation between −25 V and +25 V is observed with a maximum modulation depth of 2.5 dB. The significant modulation in the ultracompact MZM characterized by the voltage-length product of 0.23 Vcm represents to-date the highest modulation efficiency in a lithium niobate MZM (Supporting Information Note S3). Dielectric breakdown along the isolating nanogaps restricts the maximum applicable voltage which limits the achievable depth of modulation but can potentially be fully avoided by interfacing the plasmonic phase shifters with dielectric nanophotonic waveguides.[23,24,29] Capitalizing on the wide optical transparency of lithium niobate and the relatively low plasmonic losses at infrared wavelengths, spectrally broadband operation over the telecommunication wavelength bands S, C, and L (1500−1600 nm) with <6 dB modulation depth variation is demonstrated. The observed variations are caused by the wavelength dependence of the electro-optic field overlap and the shift of the operation point in the transfer function.[17] The electro-optic frequency response of the MZM is characterized from 1 MHz to 10 GHz (Figure 3c). The device exhibits a flat frequency response except a dip of −7 dB at the frequency 2.8 ± 1 GHz which is likely to be induced by nonideal impedance-matching of the used electrical feedline. The calculated device capacitance of only 3.3 fF indicates potential operation at frequencies above 900 GHz at 50 Ω resistive load ($f = 1/[2\pi RC]$), which meets the future bandwidth demands for optical integrated circuits.

DISCUSSION

By utilizing plasmonic lithium niobate technology, we demonstrated a broadband Mach−Zehnder modulator featuring a half-wave voltage-length product of 0.23 Vcm, which to date is the lowest value for a lithium niobate MZM. Spectrally broadband operation with <6 dB modulation depth variation over the optical telecommunication wavelengths (1500−1600 nm) and high-speed operation up to 10 GHz (with a potential bandwidth of 900 GHz) was demonstrated. Highly linearity modulation response is realized by passive control of the relative phase in the nonidentical waveguides forming the interferometric arms. Optical transmission and scattering losses introduced by the isolating air gap have been characterized and can potentially be further reduced by using a high-quality (monocrystalline) Au platform for the plasmonic phase shifters[18] and by eventually interfacing the plasmonic waveguides with a low-loss photonic circuit.[24] As lithium niobate provides the critical material properties for practical deployment in electro-optic modulation applications, it remains the material-of-choice for telecommunication technology. By demonstrating the possibility of realizing a lithium niobate MZM that harvests the attractive feature of plasmonics to guide both coupled electromagnetic modes and electrical signals that control their phase shift in the same metal circuitry, we enabled an exceptionally compact and efficient MZM with potential applications in next generation high speed electro-optics that can fulfill the performance-demanding needs of future data processing and quantum technologies.

METHODS

Simulations. Numerical simulations of the electro-optic response, the optical losses and the coupling efficiency of the MZM were carried out using a commercial finite element method solver (Comsol Multiphysics 5.5). For the electrostatic simulations, the cross-section of the two phase shifters is modeled with the relative permittivity ϵ_{air} = 1 of air and the strain-free static relative permittivity tensor of lithium niobate ($\epsilon_{xx} = \epsilon_{yy}$ = 27.8, ϵ_{zz} = 84.5) taken from Jazbinsek et al.[30] The electrostatic field distribution $E(x,z)$ in the phase shifter cross-section is calculated with two gold electrodes and set to ground and V_{bias}.. The electro-optically induced birefringence in LN is calculated by using the Pockels coefficients from Jazbinsek et al.[30] (with the diagonal terms, i.e., $\Delta n_{ii} = -0.5 r_{iiz} n_{ii}^3 E_z$, with $r_{xxz} = r_{yyz}$ = 10.12 pm/V and r_{zzz} = 31.45 pm/V. The optical mode analysis is conducted by considering the lateral distribution of the electro-optically modified refractive index of LN, whereas the unmodified refractive indices of Au and LN are taken from

https://doi.org/10.1021/acs.nanolett.2c00714
Nano Lett. 2022, 22, 6471−6475

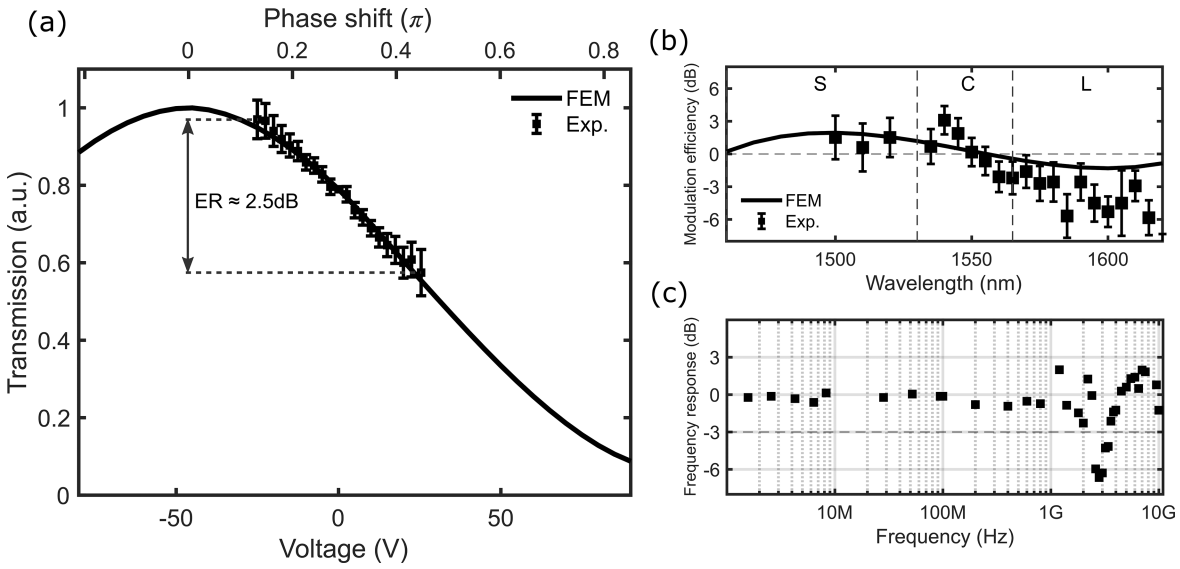

Figure 3. (a) Measured transfer function of the unbalanced Mach−Zehnder modulator, normalized by the measured transmission at 0 V. Error bars represent standard deviations and are deducted from repeated measurements. For the measured voltage range of ±25 V, an extinction ratio (ER) of 2.5 dB was measured. (b) Wavelength dependence of the modulation efficiency (at a driving voltage of V_{AC} = 15 V) normalized by the modulation efficiency measured at the free-space wavelength of 1550 nm. Error bars represent standard deviations. (c) Measured frequency response as a function of the RF modulation frequency.

Johnson and Christy[31] and Zelmon et al.[32] ($n_{xx} = n_{yy} = n_o$ = 2.211, $n_{xx} = n_e$ = 2.138 at λ_0 = 1550 nm). Possible losses introduced by imperfect Y-splitting elements are neglected and a splitting ratio of 0.5/0.5 is assumed.

Sample Fabrication. The Mach−Zehnder modulators are fabricated on commercially available *z*-cut lithium niobate substrates by electron beam lithography (using a scanning electron microscope JEOL JSM-6490LV with an acceleration voltage of 30 keV) in spin-coated 250 nm thick PMMA positive resist and a 40 nm thick conductive polymer layer (AR-PC 5090, Allresist) which serves as a metallic charge dissipation layer during the writing (electron doses varying between 200 and 250 μC/cm^2). After resist development, the devices are formed by depositing a 3 nm titanium adhesion layer and a 50 nm gold layer by thermal evaporation and subsequent 8 h lift-off. RF feed lines are patterned beforehand on the LN chip by shadow masks metal deposition (5 nm Ti/100 nm Au).

■ ASSOCIATED CONTENT

Supporting Information

The Supporting Information is available free of charge at https://pubs.acs.org/doi/10.1021/acs.nanolett.2c00714.

Optical setup for the electro-optic characterization of the plasmonic Mach−Zehnder modulators, coupled-mode theory analysis for the investigated two-wire transmission line, comparison with state-of-the-art electro-optic Mach−Zehnder modulators (PDF)

■ AUTHOR INFORMATION

Corresponding Author

Martin Thomaschewski − *Center for Nano Optics, University of Southern Denmark, DK-5230 Odense M, Denmark;* Present Address: George Washington University, 800 22nd Street NW, Washington, DC 20052, U.S.A; orcid.org/0000-0003-2545-1468; Email: thomaschewski@gwu.edu

Authors

Vladimir A. Zenin − *Center for Nano Optics, University of Southern Denmark, DK-5230 Odense M, Denmark;* orcid.org/0000-0001-5512-8288

Saskia Fiedler − *Center for Nano Optics, University of Southern Denmark, DK-5230 Odense M, Denmark*

Christian Wolff − *Center for Nano Optics, University of Southern Denmark, DK-5230 Odense M, Denmark*

Sergey I. Bozhevolnyi − *Center for Nano Optics, University of Southern Denmark, DK-5230 Odense M, Denmark;* orcid.org/0000-0002-0393-4859

Complete contact information is available at: https://pubs.acs.org/10.1021/acs.nanolett.2c00714

Notes

The authors declare no competing financial interest.

■ ACKNOWLEDGMENTS

The authors gratefully acknowledge the support from the Villum Kann Rasmussen Foundation (Award in Technical and Natural Sciences 2019).

■ REFERENCES

(1) Hunsperger, R. G. *Integrated optics*; Springer Verlag: Berlin, Heidelberg, 1995; Volume 4.

(2) Saleh, B. E.; Teich, M. C. *Fundamentals of photonics*. John Wiley & Sons, 2019.

(3) Thomaschewski, M.; Yang, Y.; Bozhevolnyi, S. I. Ultra-compact branchless plasmonic interferometers. *Nanoscale* **2018**, *10* (34), 16178−16183.

(4) Sinatkas, G.; Christopoulos, T.; Tsilipakos, O.; Kriezis, E. E. Electro-optic modulation in integrated photonics. *J. Appl. Phys.* **2021**, *130* (1), 010901.

(5) Weis, R. S.; Gaylord, T. K. Lithium niobate: Summary of physical properties and crystal structure. *Appl. Phys. A: Solids Surf.* **1985**, *37*, 191−203.

(6) Thomaschewski, M.; Bozhevolnyi, S. I. Pockels modulation in integrated nanophotonics. *Applied Physics Reviews* **2022**, *9*, 021311.

(7) Alferness, R. Polarization-independent optical directional coupler switch using weighted coupling. *Appl. Phys. Lett.* **1979**, *35*, 748−750.
(8) Bozhevolnyi, S.; Buritskii, K.; Zolotov, E.; Prokhorov, A.; Chernykh, V. A study of an electrooptic modulator utilizing coupled channel diffused waveguides in $LiNbO_3$. *Kvantovaya Elektronika* **1982**, *9*, 1808−1816.
(9) Schmidt, R.; Kaminow, I. Metal-diffused optical waveguides in $LiNbO_3$. *Appl. Phys. Lett.* **1974**, *25*, 458−460.
(10) Wang, C.; Zhang, M.; Stern, B.; Lipson, M.; Lončar, M. Nanophotonic lithium niobate electro-optic modulators. *Opt. Express* **2018**, *26*, 1547−1555.
(11) He, M.; Xu, M.; Ren, Y.; Jian, J.; Ruan, Z.; Xu, Y.; Gao, S.; Sun, S.; Wen, X.; Zhou, L.; Liu, L.; Guo, C.; Chen, H.; Yu, S.; Liu, L.; Cai, X. High-performance hybrid silicon and lithium niobate Mach−Zehnder modulators for 100 Gbit s− 1 and beyond. *Nat. Photonics* **2019**, *13* (5), 359−364.
(12) Wang, C.; et al. Integrated lithium niobate electro-optic modulators operating at CMOS-compatible voltages. *Nature* **2018**, *562*, 101−104.
(13) Boes, A.; Corcoran, B.; Chang, L.; Bowers, J.; Mitchell, A. Status and potential of lithium niobate on insulator (LNOI) for photonic integrated circuits. *Laser Photonics Rev.* **2018**, *12*, 1700256.
(14) Rao, A.; Fathpour, S. Compact lithium niobate electrooptic modulators. *IEEE J. Sel. Top. Quantum Electron.* **2018**, *24*, 1−14.
(15) Mahmoud, M.; Cai, L.; Bottenfield, C.; Piazza, G. Lithium niobate electro-optic racetrack modulator etched in Y-Cut LNOI platform. *IEEE Photonics J.* **2018**, *10*, 1−10.
(16) Thomaschewski, M.; Zenin, V. A.; Wolff, C.; Bozhevolnyi, S. I. Plasmonic monolithic lithium niobate directional coupler switches. *Nat. Commun.* **2020**, *11*, 748.
(17) Thomaschewski, M.; Wolff, C.; Bozhevolnyi, S. I. High-speed plasmonic electro-optic beam deflectors. *Nano Lett.* **2021**, *21* (9), 4051−4056.
(18) Lebsir, Y.; Boroviks, S.; Thomaschewski, M.; Bozhevolnyi, S.I.; Zenin, V. A. Ultimate Limit for Optical Losses in Gold, Revealed by Quantitative Near-Field Microscopy. *Nano Letters* **2022**, *22*, 5759−5764.
(19) Lin, H.; Ogbuu, O.; Liu, J.; Zhang, L.; Michel, J.; Hu, J. Breaking the energy-bandwidth limit of electrooptic modulators: theory and a device proposal. *Journal of Lightwave Technology* **2013**, *31* (24), 4029−4036.
(20) Ebbesen, T. W.; Genet, C.; Bozhevolnyi, S. I. Surface-plasmon circuitry. *Phys. Today* **2008**, *61*, 44−50.
(21) Thomaschewski, M.; Yang, Y.; Wolff, C.; Roberts, A.; Bozhevolnyi, S. I. On-chip detection of optical spin-orbit interactions in plasmonic nanocircuits. *Nano Lett.* **2019**, *19*, 1166−1171.
(22) Yezekyan, T.; Thomaschewski, M.; Bozhevolnyi, S. I. On-Chip Ge Photodetector Efficiency Enhancement by Local Laser-Induced Crystallization. *Nano Lett.* **2021**, *21* (18), 7472−7478.
(23) Melikyan, A.; et al. High-speed plasmonic phase modulators. *Nat. Photonics* **2014**, *8* (4), 229−233.
(24) Haffner, C.; et al. All-plasmonic Mach−Zehnder modulator enabling optical high-speed communication at the microscale. *Nat. Photonics* **2015**, *9* (8), 525−528.
(25) Damgaard-Carstensen, C.; Thomaschewski, M.; Ding, F.; Bozhevolnyi, S. I. Electrical Tuning of Fresnel Lens in Reflection. *ACS Photonics* **2021**, *8* (6), 1576−1581.
(26) Gramotnev, D. K.; Bozhevolnyi, S. I. Plasmonics beyond the diffraction limit. *Nat. Photonics* **2010**, *4* (2), 83−91.
(27) Sorger, V. J.; Oulton, R. F.; Ma, R. M.; Zhang, X. Toward integrated plasmonic circuits. *MRS Bull.* **2012**, *37* (8), 728−738.
(28) Davis, T. J.; Gómez, D. E.; Roberts, A. Plasmonic circuits for manipulating optical information. *Nanophotonics* **2016**, *6* (3), 543−559.
(29) Thraskias, C. A.; et al. Survey of photonic and plasmonic interconnect technologies for intra-datacenter and high-performance computing communications. *IEEE Communications Surveys & Tutorials* **2018**, *20* (4), 2758−2783.
(30) Jazbinsek, M.; Zgonik, M. Material tensor parameters of $LiNbO_3$ relevant for electro- and elasto optics. *Appl. Phys. B: Lasers Opt.* **2002**, *74*, 407−414.
(31) Johnson, P. B.; Christy, R.-W. Optical constants of the noble metals. *Phys. Rev. B* **1972**, *6*, 4370.
(32) Zelmon, D. E.; Small, D. L.; Jundt, D. Infrared corrected Sellmeier coefficients for congruently grown lithium niobate and 5 mol.% magnesium oxide−doped lithium niobate. *J. Opt. Soc. Am. B* **1997**, *14*, 3319−3322.

https://doi.org/10.1021/acs.nanolett.2c00714
Nano Lett. 2022, 22, 6471−6475

Supplementary information for

PLASMONIC LITHIUM NIOBATE MACH-ZEHNDER MODULATORS

Martin Thomaschewski, Saskia Fiedler, Vladimir Zenin, Christian Wolff, and Sergey I. Bozhevolnyi

Center for Nano Optics, University of Southern Denmark, Campusvej 55, DK-5230 Odense M, Denmark

S1: Optical setup for the electro-optic characterization of the plasmonic Mach-Zehnder modulators

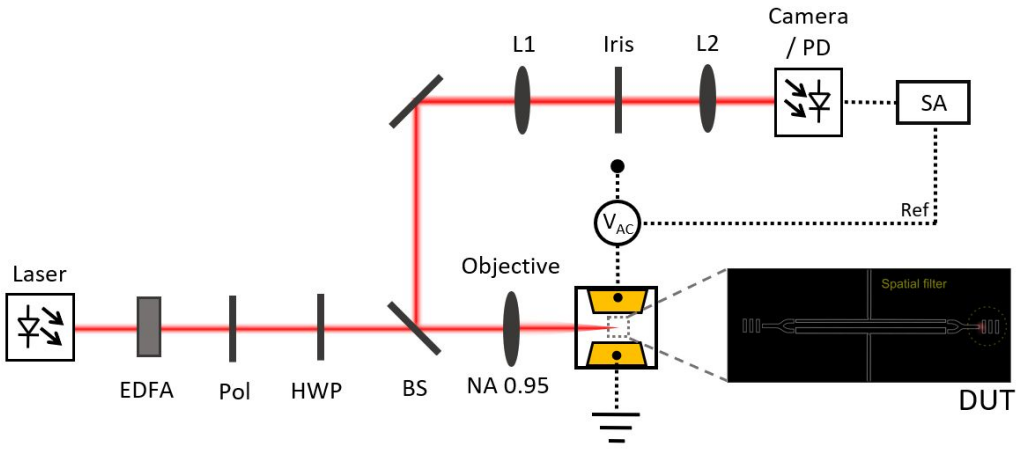

Figure S1 Schematic of the setup used for the electro-optic characterization of the plasmonic lithium niobate Mach-Zehnder modulators (MZM). The optical path is illustrated as red lines and the electrical wiring as dashed black lines. A linearly polarized light beam from a wavelength tunable IR laser is used as an excitation source. After amplifying the beam with an Erbium Doped Fiber Amplifier (EDFA) and passing a polarizer (P) and a half-wave plate (HWP), the laser beam is focused on the sample surface at normal incidence with an IR-objective (×100 magnification, NA = 0.95). The scattered optical signal is collected by the same objective. A spatial filter selects the scattered signal at the output grating before the signal is analyzed by an infrared camara or a high-speed photodiode. A detailed description of the RF measurement used for characterizing the frequency response of the device can be found in [3].

S3: Coupled Mode formalism

The performance of our device can be well explained within the coupled mode formalism.[1,2] Here we will continue using the variables and theoretical description introduced in our previous work.[3] However, in this case, the waveguides are not identical, therefore it is better to introduce the following auxiliary variables:

$$\kappa_{\mathrm{n}} \equiv \frac{1}{\Delta\beta_{\mathrm{n}}} = \frac{2\kappa}{\Delta\beta}, \qquad \delta = \sqrt{1+\kappa_{\mathrm{n}}{}^{2}}, \tag{1.1}$$

where κ_{n} is the normalized coupling coefficient dependent on the waveguide separation. With the above variables, the propagation constants of even and odd modes are

$$\begin{cases} \beta_{\mathrm{even}} = \beta_{\mathrm{avg}} + \frac{\Delta\beta}{2}\delta \\ \beta_{\mathrm{odd}} = \beta_{\mathrm{avg}} - \frac{\Delta\beta}{2}\delta \end{cases} \tag{1.2}$$

Thus, the normalized coupling coefficient can be determined from the propagation constants of each individual waveguide and hybrid even and odd modes:

$$\kappa_{\mathrm{n}} = \sqrt{\left(\frac{\beta_{\mathrm{even}} - \beta_{\mathrm{odd}}}{\Delta\beta}\right)^{2} - 1} \tag{1.3}$$

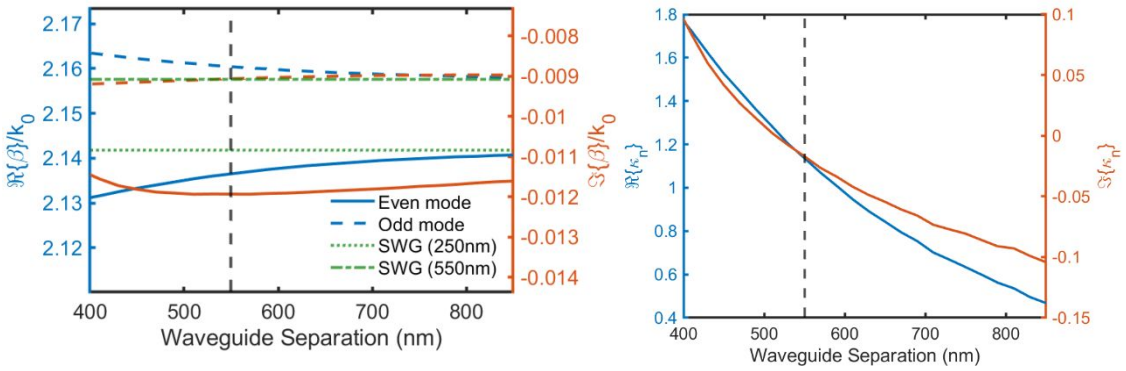

Figure S2. Coupled-mode analysis of the plasmonic phase shifters as a function of the edge-to-edge waveguide separation with two parallel Au nanowires with a width of w_1 = 250 nm and w_2 = 550 nm at zero applied voltage. The demonstrated electro-optic phase shifter has an edge-to-edge separation of 550 nm (vertical dash line). **(a)** Mode effective indices of the odd (solid) and even modes (dashed), compared to the ones of each individual waveguide modes (dotted and dash-dotted lines). **(b)** Normalized coupling coefficient, κ_n, as a function of the waveguide separation.

The evolution of the electromagnetic field in the system is the following:

$$\begin{aligned}\{\mathbf{E}(x,y,z),\mathbf{H}(x,y,z)\} = {} & [\{\mathbf{E_1}(x,z),\mathbf{H_1}(x,z)\}\alpha_{\text{even}} + \{\mathbf{E_2}(x,z),\mathbf{H_2}(x,z)\}]S_{\text{even}}e^{j\beta_{\text{even}}y} \\ & + [\{\mathbf{E_1}(x,z),\mathbf{H_1}(x,z)\}\alpha_{\text{odd}} + \{\mathbf{E_2}(x,z),\mathbf{H_2}(x,z)\}]S_{\text{odd}}e^{j\beta_{\text{odd}}y},\end{aligned} \tag{1.4}$$

where S_{even} and S_{odd} are constants, determined from initial boundary conditions, and

$$\begin{cases}\alpha_{\text{even}} = \frac{1}{\kappa_n}(1+\delta) \\ \alpha_{\text{odd}} = \frac{1}{\kappa_n}(1-\delta)\end{cases} \tag{1.5}$$

One can already notice that, in the case of weak coupling ($\kappa_n \to 0$), $\beta_{\text{even}} \to \beta_1$, $\beta_{\text{odd}} \to \beta_2$, $\alpha_{\text{even}} \to \infty$, $\alpha_{\text{odd}} \to 0$, that is, even and odd modes simplify to being simply the modes of individual waveguides.

The above eq. (1.3) can be rewritten as

$$\{\mathbf{E}(x,y,z),\mathbf{H}(x,y,z)\} = A_1(y)\{\mathbf{E_1}(x,z),\mathbf{H_1}(x,z)\} + A_2(y)\{\mathbf{E_2}(x,z),\mathbf{H_2}(x,z)\}, \tag{1.6}$$

where

$$\begin{cases}A_1(y) = e^{j\beta_{\text{avg}}y}\left(\alpha_{\text{even}}S_{\text{even}}e^{j\frac{\Delta\beta}{2}\delta y} + \alpha_{\text{odd}}S_{\text{odd}}e^{-j\frac{\Delta\beta}{2}\delta y}\right) \\ A_2(y) = e^{j\beta_{\text{avg}}y}\left(S_{\text{even}}e^{j\frac{\Delta\beta}{2}\delta y} + S_{\text{odd}}e^{-j\frac{\Delta\beta}{2}\delta y}\right)\end{cases} \tag{1.7}$$

In our MZM device, the light is coupled into a single-waveguide mode of the input Y-branch. Then the power is split equally into both arms (w = 400 nm each) at the symmetric Y-branch output (i.e., it is transformed into the even mode), and coupled via the air gap into each of waveguides (w_1 = 250 nm and w_2 = 550 nm). Because these waveguides are evenly different from the Y-branch waveguide (i.e., one is 150-nm narrower and another is 150-nm wider), it is reasonable to assume the same coupling efficiency via the air gap. Then, without losing generality, one can assume that the excited fields in each waveguide are

$$A_1(0) = A_2(0) = 1 \text{ a.u.} \tag{1.8}$$

These fields change upon propagation according to the above eq. (1.7) and reach the input of the second output symmetric Y-branch. The output Y-branch does the same as the first one: it converts even mode of its two-waveguide part into a single-waveguide mode, while the odd mode is scattered out and back reflected. Thus, the overall MZM output transmittance, neglecting coupling losses through air gaps, will be the following:

$$T = \left|\frac{A_1(L) + A_2(L)}{2}\right|^2 \tag{1.9}$$

Using initial condition (1.8) with (1.7), one can find

$$\begin{cases} S_{\text{even}} = \dfrac{1 - \alpha_{\text{odd}}}{\alpha_{\text{even}} - \alpha_{\text{odd}}} = \dfrac{\delta - 1 + \kappa_{\text{n}}}{2\delta} \\ S_{\text{odd}} = \dfrac{\alpha_{\text{even}} - 1}{\alpha_{\text{even}} - \alpha_{\text{odd}}} = \dfrac{\delta + 1 - \kappa_{\text{n}}}{2\delta} \end{cases} \tag{1.10}$$

Inserting this into (1.9) will result in the following expression:

$$\begin{aligned} T &= e^{-2\text{Im}\{\beta_{\text{avg}}L\}}\left|\frac{\alpha_{\text{even}} + 1}{2} S_{\text{even}} e^{j\frac{\Delta\beta}{2}\delta L} + \frac{\alpha_{\text{odd}} + 1}{2} S_{\text{odd}} e^{-j\frac{\Delta\beta}{2}\delta L}\right|^2 \\ &= e^{-2\text{Im}\{\beta_{\text{avg}}L\}}\left|\frac{1 + \delta + \kappa_{\text{n}}}{2\kappa_{\text{n}}}\frac{\delta - 1 + \kappa_{\text{n}}}{2\delta} e^{j\frac{\Delta\beta}{2}\delta L} + \frac{1 - \delta + \kappa_{\text{n}}}{2\kappa_{\text{n}}}\frac{\delta + 1 - \kappa_{\text{n}}}{2\delta} e^{-j\frac{\Delta\beta}{2}\delta L}\right|^2 \\ &= e^{-2\text{Im}\{\beta_{\text{avg}}L\}}\left|\frac{\delta + \kappa_{\text{n}}}{2\delta} e^{j\frac{\Delta\beta}{2}\delta L} + \frac{\delta - \kappa_{\text{n}}}{2\delta} e^{-j\frac{\Delta\beta}{2}\delta L}\right|^2 \\ &= e^{-2\text{Im}\{\beta_{\text{avg}}L\}}\left|\cos\left(\frac{\Delta\beta}{2}\delta L\right) + j\frac{\kappa_{\text{n}}}{\delta}\sin\left(\frac{\Delta\beta}{2}\delta L\right)\right|^2 \end{aligned} \tag{1.11}$$

In the case of negligibly small coupling ($\kappa_{\text{n}} = 0$), the transmittance is simply

$$T_0 = e^{-2\text{Im}\{\beta_{\text{avg}}L\}}\left|\cos\left(\frac{\Delta\beta}{2}L\right)\right|^2. \tag{1.12}$$

The first factor $e^{-2\text{Im}\{\beta_{\text{avg}}L\}}$ is simply the average amplitude loss due to the absorption in the waveguides. Then, by changing the applied voltage, one can tune $\Delta\beta$ to modulate the output between maxima and minima. In our MZM device, the length L is chosen to be in the quadrature point, that is, $\text{Re}\left\{\frac{\Delta\beta_0}{2}L\right\} = \frac{\pi}{4}$, $L = \frac{\pi}{2\text{Re}\{\Delta\beta_0\}}$, where Δ

β_0 is the value at zero applied voltage. The minima and, thus, the modulation extinction ratio is limited by uneven losses in each waveguide, that is,

$$\frac{T_{0,\max}}{T_{0,\min}} \approx \left|\cos\left(\frac{j\mathrm{Im}\{\Delta\beta\}}{2}L\right)\right|^{-2} = \left|\cosh\left(\frac{1}{2}\mathrm{Im}\{\Delta\beta\}L\right)\right|^{-2} = \left|\cosh\left(\frac{1}{2}\mathrm{Im}\{\Delta\beta\}L\right)\right|^{-2} = \left|\cosh\left(\frac{2\pi\mathrm{Im}\{\Delta\beta\}}{\mathrm{Re}\{\Delta\beta_0\}}\right)\right|^{-2} \quad (1.13)$$

However, in the real device it is necessary to place both waveguides close in order to reduce the modulation voltage, which leads to the non-zero coupling. It is reasonable to assume, that it is the coupling coefficient $\kappa = \frac{\Delta\beta\kappa_n}{2}$, which stays nearly constant during voltage tuning, since it is a measure of the field overlap between mode profiles of each waveguide modes. The validity of this assumption is confirmed by rigorously calculating the propagation constants for individual waveguide modes and those of even/odd supermodes for our separation of 550 nm as a function of the applied voltage (Figure S3a), and then calculating the coupling coefficient (Figure S3b).

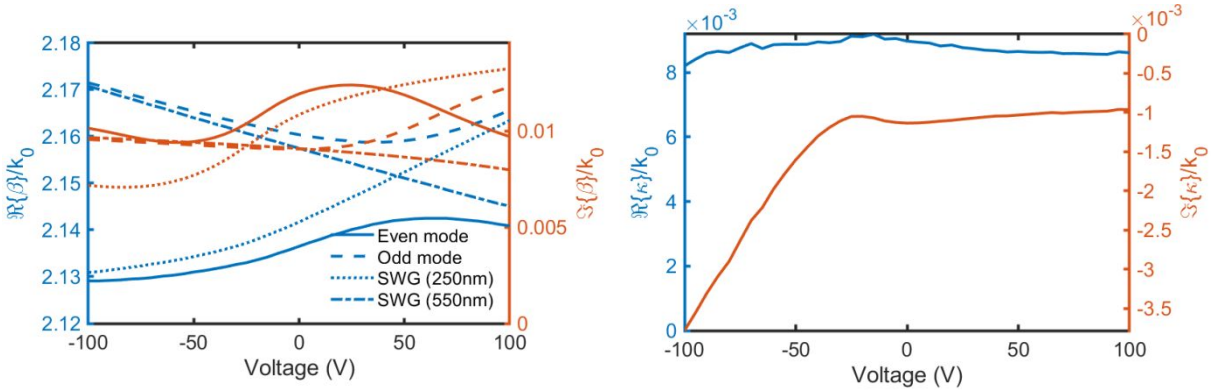

Figure S3. **(a)** Mode effective indices of the odd (solid) and even modes (dashed), compared to the ones of each individual waveguide modes (dotted and dash-dotted lines) as a function of the applied voltage. **(b)** The coupling coefficient κ as a function of the applied voltage.

The effect of coupling [evaluation of the equation (1.11), using both the approximate model with a constant coupling coefficient κ and a precise model with its voltage dependance, is shown in Figure S4 below. It becomes thereby clear, that there is a trade-off in the proposed device: the operation voltage can be reduced with a price of the reduced modulation depth.

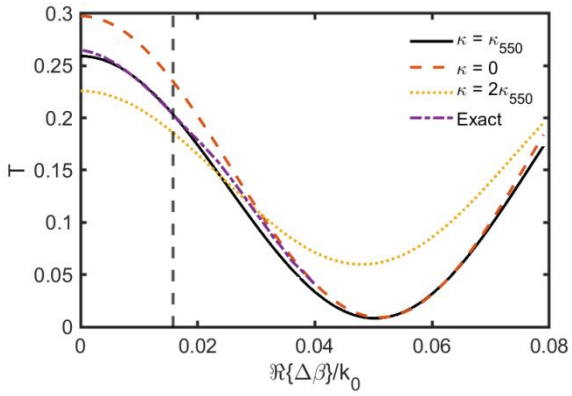

Figure S4. Total transmission as a function of the voltage-dependent waveguide effective mode index modification, $\mathrm{Re}\{\Delta\beta/k_0\}$, estimated for the actual coupling coefficient of κ_{550} at 550 nm waveguide separation (solid), zero coupling coefficient $\kappa = 0$ (dashed), and for twice as large coupling coefficient, $\kappa = 2\ \kappa_{550}$ (dotted), assuming voltage-independent coupling coefficient. Results for the rigorous simulations with voltage-dependent κ_{550} are plotted with dash-dotted line.

S3: Comparison with state-of-the-art electro-optic Mach-Zehnder modulators

Material Platform	**r_{33} / pm·V^{-1}**	**Thermal stability**	**$V_\pi \cdot L$ / V · cm**	**Device footprint**	**Phase shifter Insertion loss / dB**	**Reference**
LN	**30**	+	22	-	< 3	[4]
LN	30	+	6.4	+/-	0.3	[5]
PZT	61	+/-	3.2	+/-	0.05	[6]
LN	30	+	2.2	+/-	0.4	[7]
LN	30	+	1.8	+/-	1.5	[8]
LN (Plasmonic)	**30**	**+**	**0.23**	+	**19.5**	**Our work**
EOP M3	91	-	0.11	-	2.5	[9]
EOP YLD-124 (Plasmonic)	100	-	0.012	+	6	[10]
EOP DLD-164 (Plasmonic)	180	-	0.006	+	2.5	[11]

Table S1. Comparison of state-of-the-art electro-optic Pockels MZM modulators ordered by the half-wave voltage-length product. The material platform used in the individual modulator devices are lithium niobite (LN), Lead zirconate titanate (PZT) and electro-optic polymers (EOP). The insertion loss is defined by the waveguide propagation loss in the phase-shifter section. The thermal stability is classified by the threshold temperature T_t of structural phase transition in the material to be low (-) at T_t< 100 °C, medium (+/-) at 100 °C < T_t < 300 °C or high (+) at T_t > 300 °C. The footprint refers to the surface area occupied by a structure on the chip to be small (+) with the area A < 1 mm^2, medium (+/-) with 1 mm^2 < A < 1 cm^2 or large (-) with A >1 cm^2.

References

[1] Alferness, R. Guided-wave devices for optical communication. IEEE J. Quantum Elect. 17, 946–959 (1981).

[2] Kogelnik, H. and Schmidt R. Switched directional couplers with alternating ΔB. IEEE J. Quantum Elect. 12, 396–401 (1976).

[3] Thomaschewski, M., Zenin, V.A., Wolff, C. et al. Plasmonic monolithic lithium niobate directional coupler switches. Nat. Commun. 11, 748 (2020)

[4] Thorlabs, Lithium Niobate Electro-Optic Modulators, Fiber-Coupled, Retrieved May 18, 2022, from https://www.thorlabs.com/newgrouppage9.cfm?objectgroup_id=3918

[5] Weigel, P. O. *et al.* Bonded thin film lithium niobate modulator on a silicon photonics platform exceeding 100 GHz 3-dB electrical modulation bandwidth. *Opt. Express* **26**, 23728-23729 (2018).

[6] Alexander, K. *et al.* Nanophotonic Pockels modulators on a silicon nitride platform. *Nat. Commun.* **9**, 3444 (2018).

[7] Wang, C. *et al.* Integrated lithium niobate electro-optic modulators operating at CMOS-compatible voltages. *Nature* **562**, 101–104 (2018).

[8] Wang, C., Zhang, M., Stern, B., Lipson, M., and Lončar, M. Nanophotonic lithium niobate electro-optic modulators. *Opt. Express* **26**, 1547-1555 (2018).

[9] Alloatti, L. *et al.* 100 GHz silicon–organic hybrid modulator. *Light Sci. Appl.* **3**, e173 (2014).

[10] Ayata, M. *et al.* High-speed plasmonic modulator in a single metal layer. *Science* **358**, 630–632 (2017).

[11] Haffner, C. *et al.* All-plasmonic Mach–Zehnder modulator enabling optical high-speed communication at the microscale. *Nat. Photonics* **9**, 525–528 (2015).